

# Desiccation cracks provide evidence of lake drying on Mars, Sutton Island member, Murray formation, Gale Crater

N. Stein<sup>1</sup>, J.P. Grotzinger<sup>1</sup>, J. Schieber<sup>2</sup>, N. Mangold<sup>3</sup>, B. Hallet<sup>4</sup>, H. Newsom<sup>5</sup>, K.M. Stack<sup>6</sup>, J.A. Berger<sup>7</sup>, L. Thompson<sup>8</sup>, K.L. Siebach<sup>9</sup>, A. Cousin<sup>10</sup>, S. Le Mouélic<sup>3</sup>, M. Minitti<sup>11</sup>, D.Y. Sumner<sup>12</sup>, C. Fedo<sup>13</sup>, C.H. House<sup>14</sup>, S. Gupta<sup>15</sup>, A.R. Vasavada<sup>6</sup>, R. Gellert<sup>16</sup>, R. C. Wiens<sup>17</sup>, J. Frydenvang<sup>18</sup>, O. Forni<sup>10</sup>, P.Y. Meslin<sup>10</sup>, V. Payré<sup>19</sup>, and E. Dehouck<sup>10</sup>

<sup>1</sup>Division of Geological and Planetary Sciences, California Institute of Technology, Pasadena, California 91125, USA

<sup>2</sup>Department of Geological Sciences, Indiana University, Bloomington, Indiana 47405, USA

<sup>3</sup>Laboratoire Planétologie Géodynamique, UMR6112 CNRS/Université Nantes, Nantes, France

<sup>4</sup>Department of Earth and Space Sciences, University of Washington, Seattle, Washington 98105, USA

<sup>5</sup>Institute of Meteoritics and Department of Earth and Planetary Sciences, University of New Mexico, Albuquerque, New Mexico 87131, USA

<sup>6</sup>Jet Propulsion Laboratory, California Institute of Technology, Pasadena, California 91109, USA

<sup>7</sup>Department of Earth Sciences, University of Western Ontario, London, ON N6A 5B7, Canada

<sup>8</sup>Planetary and Space Science Centre, University of New Brunswick, NB E3B 5A3, Canada

<sup>9</sup>Department of Geosciences, Stony Brook University, Stony Brook, New York 11795, USA

<sup>10</sup>Institut de Recherche en Astrophysique et Planétologie, Université de Toulouse, UPS-CNRS-OMP, Toulouse, France

<sup>11</sup>Planetary Science Institute, Tucson, Arizona 85719, USA

<sup>12</sup>Department of Earth and Planetary Sciences, University of California, Davis, California 95616, USA

<sup>13</sup>Department of Earth and Planetary Sciences, University of Tennessee, Knoxville, Tennessee 37996, USA

<sup>14</sup>Department of Geosciences and Penn State Astrobiology Research Center, The Pennsylvania State University, University Park, Pennsylvania 16802, USA

<sup>15</sup>Department of Earth Science and Engineering, Imperial College London, London SW7 2AZ, UK

<sup>16</sup>Department of Physics, University of Guelph, Guelph, ON N1G 2W1, Canada

<sup>17</sup>Los Alamos National Laboratory, Los Alamos, New Mexico 87544, USA

<sup>18</sup>Natural History Museum of Denmark, University of Copenhagen, Copenhagen, Denmark

<sup>19</sup>Université de Lorraine, 54000 Nancy, France

## ABSTRACT

**Mars Science Laboratory (MSL) Curiosity rover data are used to describe the morphology of desiccation cracks observed in ancient lacustrine strata at Gale crater, Mars, and to interpret their paleoenvironmental setting. The desiccation cracks indicate subaerial exposure of lacustrine facies in the Sutton Island member of the Murray formation. In association with ripple cross-stratification and possible eolian cross-bedding, these facies indicate a transition from longer-lived perennial lakes recorded by older strata to younger lakes characterized by intermittent exposure. The transition from perennial to episodically exposed lacustrine environments provides evidence for local to regional climate change that can help constrain Mars climate models.**

## INTRODUCTION

Reconstructions of ancient habitable environments on Mars increasingly depend on detailed analysis of sedimentary facies recording aqueous environments. Over the past decade, the Mars Exploration Rover Opportunity encountered ancient eolian, fluvial, and lacustrine environments deposited in hypersaline, acidic, sulfate- and hematite-enriched playas formed in interdune depressions at Meridiani Planum (e.g. Grotzinger et al., 2005). This setting contrasts with the clay- and magnetite-bearing, moderate pH, perennial lacustrine facies in Gale crater (Grotzinger et al., 2014, 2015; Hurowitz et al., 2017; Rampe et al., 2017). Suites of sedimentary structures, facies associations, and authigenic and diagenetic mineral assemblages were essential to recognize these paleoenvironmental settings. Previously, potential martian desiccation cracks

were identified in multiple sedimentary deposits from orbit (e.g., El-Maarry et al., 2014) and *in situ* by rovers (Grotzinger et al., 2005, 2014).

The kilometers-thick sedimentary succession in Gale crater provides an opportunity to observe changes in surface environments over extended periods in martian history. Studies of basal strata in the informally named Murray formation demonstrated the presence of long-lived perennial lakes in Gale crater at ca. 3.6–3.2 Ga (Grotzinger et al., 2014, 2015; Hurowitz et al., 2017). Recent facies observations at higher stratigraphic levels (Fedo et al., 2017) may record an evolution of the environment over time. Here we present *in situ* evidence for lithified desiccation cracks in the Murray formation, indicating that the lakes may have partially dried in its younger history.

During Sols 1555–1571, Curiosity investigated a series of distinctive centimeter-scale

reticulate ridges on the surfaces of several slabs of rock that expose bedding planes in the Sutton Island member of the Murray formation. Their morphology and composition is characterized to determine if they formed via desiccation and to examine implications for the deposition of associated strata.

## GEOLOGIC SETTING

As of Sol 1700, the Curiosity rover has explored more than 200 m of strata consisting of fluvial, deltaic, lacustrine, and eolian sediments (Williams et al., 2013; Grotzinger et al., 2014, 2015; Banham et al., 2016; Edgar et al., 2017) represented by the Bradbury group, the interfingering and overlying Murray formation (Mount Sharp group), and the unconformably overlying Stimson formation (Siccar Point group) (Fig. 1). The first ~25-m-thick Murray interval consists dominantly of finely laminated mudstones with minor siltstones and sandstones of lacustrine origin (Grotzinger et al., 2015). It is overlain by an ~25-m-thick interval with decimeter- to meter-scale cross-stratification that suggests sediment transport as large bedforms or in channels (Fedo et al., 2017), followed by >30 m of finely laminated red/purple-hued mudstone with intervals of very fine sandstone, consistent with sediment accumulation in subaqueous lacustrine environments (Grotzinger et al., 2015; Fedo et

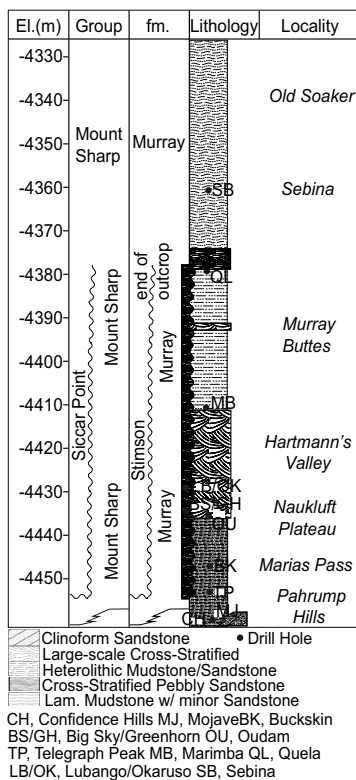


**Figure 1.** Stratigraphic column for the sedimentary facies of the Murray formation, Mars. Old Soaker (OS) rock slab is in the heterolithic facies of the Sutton Island member of the Murray formation. El.—elevation; Lam.—laminated.

al., 2017). These younger strata, comprising the Sutton Island member of the Murray formation, expose broken and tilted slabs of bedrock, including finely laminated red mudstones, centimeter-scale ripple cross-laminated mudstone, decimeter-scale cross-stratification, and massively bedded intervals of siltstone (Fedó et al. 2017).

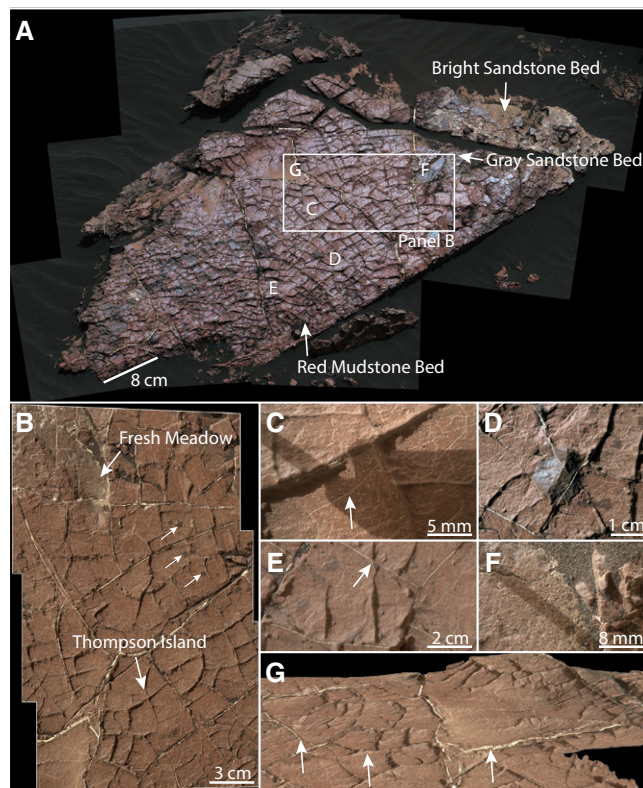
## OLD SOAKER CAMPAIGN

The focus of the investigation is an ~80-cm-long, 40-cm-wide rock slab called “Old Soaker” (OS) that exposes a bedding plane with a red surface marked by a network of ridges that form polygons (Fig. 2A). The red mudstone is ~1 cm thick and overlies a gray sandstone bed containing bedding-parallel seams of calcium sulfate ( $\text{CaSO}_4$ ). OS and a similar nearby slab called “Squid Cove” (SC) were imaged with the Mast Camera (Mastcam) and the Mars Hand Lens Imager (MAHLI) to characterize the geometry and fill of the ridges. Their elemental compositions were examined with the rover’s ChemCam Laser Induced Breakdown Spectrometer (LIBS) and Alpha-Particle X-Ray Spectrometer (APXS).

## Methods

The geometries of the polygonal ridges were determined using MAHLI images to evaluate whether their shape is consistent with desiccation. Images of ridges and their junctions were

**Figure 2.** Mastcam (sol 1555) and Mars Hand Lens Imager (MAHLI) images of Old Soaker (OS) rock slab, Mars. **A:** A network of raised ridges forms closed polygons on a red bed on OS. White calcium-sulfate ( $\text{CaSO}_4$ ) veins follow many of the ridges. Ridgeless gray beds underlie the red bed. **B:** Mosaic of nadir MAHLI images of OS. Arrows point to alpha-particle X-ray spectrometer (APXS) targets shown in Table 2, and examples of dark spots. Illumination from upper left. **C:** Partly shadowed MAHLI image of Thompson Island. White arrow denotes a sub-millimeter-wide fracture in a polygon. **D:** MAHLI image shows ridges terminating on a gray patch. Illuminated from left. **E:** MAHLI image shows a  $\text{CaSO}_4$  vein cross-cutting a ridge (arrow). Illuminated from upper left. **F:** MAHLI image of the gray bed (target Fresh Meadow). Illuminated from upper left. **G:** 3-D view of the red bed showing ridges tapering off into a depression. Left arrow:  $\text{CaSO}_4$  vein on side of ridge; middle arrow: typical polygon-forming ridge; right arrow:  $\text{CaSO}_4$  vein.



traced to calculate vertex angle distributions, widths of ridges and the polygons they form, and ridge surface area. A three-dimensional (3-D) model of OS was generated from 76 MAHLI images processed using photogrammetry software. The grain sizes of the red and gray beds were measured with ~16  $\mu\text{m}/\text{pixel}$  MAHLI images.

## RESULTS

### Morphology of the Ridges and Surrounding Beds

The red surfaces of OS and SC are covered by networks of arcuate ridges with up to 5 mm of positive relief that define predominantly four-sided and some five-sided, 0.5–3.5-cm-wide polygons (Figs. 2B and 3A). Red surfaces of adjacent slabs also show raised ridges spanning an area of a few square meters. The ridges range in length from a few centimeters to ~0.3 m and mostly meet orthogonally, forming T-junctions (Fig. 3B). The ridges are made of red-to-gray sediment similar in color to the surrounding bed (Figs. 2B and 2C) and comprise ~20% of OS’s surface. No grains in the ridges or surrounding surface are resolved in MAHLI images (Fig. 2C), indicating a maximum grain size of coarse silt.  $\text{CaSO}_4$  veins distinct from ridge material follow most, but not all, of the ridges (Figs. 2B and 2C) and in some cases cross-cut the ridges (e.g., Fig. 2E). Sub-millimeter-wide fractures occur within

the polygons (Fig. 2C). Gray, semi-circular, millimeter-scale patches dot the red beds on OS and SC. They can show raised relief and in places are cross-cut by veins (Figs. 2B and 2D).

Some very fine sand grains and millimeter-scale concretions or embedded grains are visible in MAHLI images of the gray bed at OS (Fig. 2F). The ridges taper off within millimeter-scale depressions in the red mudstone at OS (Fig. 2G). Fractures associated with the ridges of the SC slab penetrate the red mudstone and terminate at the boundary with the underlying gray sandstone (Fig. 4). The gray beds appear to lack ridges (Figs. 2A and 2F).

### Composition Measurements at Old Soaker and Squid Cove

ChemCam analysis of OS identified three distinct bed compositions (Fig. 2A): (1) a low-most bright sandstone with no ridges and a

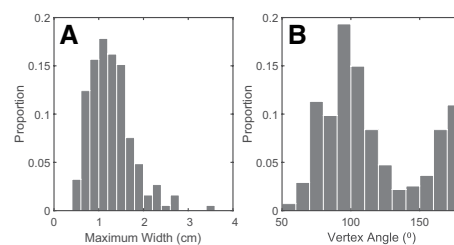


**Figure 3.** Distribution of the maximum width of polygons (A) and vertex angles (B) formed by ridges on Old Soaker rock slab, Mars.

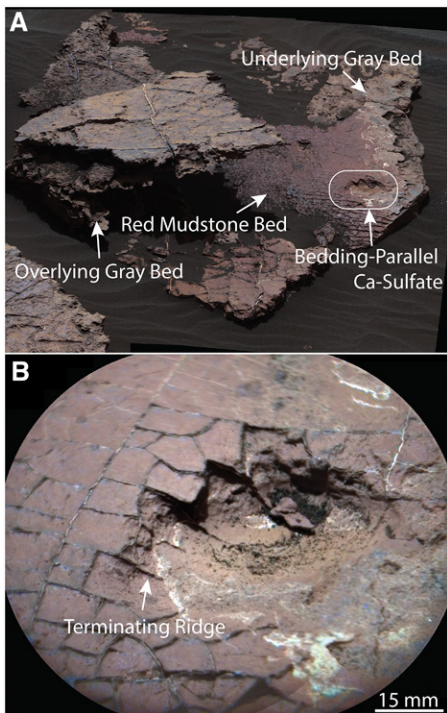


**Figure 4. A: Mastcam image of Squid Cove (SC) rock slab, Mars (sol 1555). Ridges form polygons in a thin red bed. B: Colorized ChemCam RMI mosaic of the contact between the red and gray beds on SC (white box, frame A). Fractures penetrate the red bed and terminate at the boundary with the underlying gray bed. Illumination from upper left.**

composition consistent with cementation of sandstones by calcium sulfates; (2) a gray bed with comparatively high  $K_2O$  abundance relative to the bright sandstone (1.5–2.5 wt%); and (3) an overlying red mudstone compositionally similar to other Murray mudstones (Table 1) (Mangold et al., 2017). APXS measurements of OS show that the red mudstone bed is similar in composition to average Murray bedrock, but is two to three times richer in Cl (2–3 wt%) and Br (1150–1430 ppm). The gray bed (target “Fresh Meadow”) is distinct from the overlying red bed, with relatively

enriched  $K_2O$ ,  $SO_3$ ,  $Na_2O$ , and  $FeO_T$  and depleted  $TiO_2$ ,  $SiO_2$ , and  $Al_2O_3$  (Table 2).

ChemCam observation points on the ridges validate that their composition is distinct from  $CaSO_4$  vein fill and close to that of the gray bed, with lower  $Al_2O_3$  and  $SiO_2$ , high H emission lines, and higher  $K_2O$  abundances than the red bed. The presence of strong H lines on the ridges indicates the presence of a significant component of hydrous phases absent from the red layer. The dark patches (target “Gilley Field”; Table 1) in the red bed are enriched in FeO (up to 27 wt%) and MnO (0.7 wt%) relative to the surrounding rock. The bright veins are similar to  $CaSO_4$  veins encountered since the beginning of the mission (Table 1) (Nachon et al., 2017).

## DISCUSSION

Proposed formation mechanisms for the ridges must account for several observations: (1) ridges form polygonal networks with T-junctions and continuous arcuate shapes; (2) the ridges in the red mudstone beds correspond to fractures that penetrate those beds; (3) the fractures are restricted to the red beds and terminate at the boundary with coarser underlying material; (4) the fractures are filled with very fine-grained sediment; (5)  $CaSO_4$  veins run along many but not all of the ridges, in some cases cross-cut the ridges, and, unlike the ridges, cut all beds in exposed cross sections; and (6) the ridges are compositionally similar to the underlying gray bed. The most likely fracturing mechanisms include desiccation, syneresis, and hydraulic fracturing.

### Origin of the Ridges

Shrinkage cracks form in response to tensile stresses within sediment that result from contraction due to moisture or heat loss (Shorlin et al., 2000). When stress exceeds local tensile strength, materials fracture and cracks begin to grow orthogonal to the direction of maximum tensile stress, typically resulting in a polygonal pattern (Sletten et al., 2003). In uniform material, new

cracks will turn to converge with other cracks orthogonally, resulting in junctions mostly near  $90^\circ$  (Shorlin et al., 2000) as observed at OS and SC (Fig. 3). Abundant T-junctions show that sediments dried to completion, possibly in a single event, rather than undergoing multiple wetting and drying cycles that tend to form  $120^\circ$  junctions (Goehring et al., 2010).

Desiccation cracks form at the sediment-air interface and are preserved in the rock record through sediment infill from overlying strata (Plummer and Gostin, 1981). The compositional and color similarity of the ridges to the average Murray formation, which is predominantly comprised of silt-sized grains or smaller, suggests that the ridges are comprised of sediment. Ridge-forming sediment at OS and SC is indistinguishable from the surrounding bed based on grain size alone, so this observation is not definitive evidence for sediment infill from an overlying bed.

Sulfate-mineralized fractures attributed to hydraulic fracturing are prevalent throughout the Murray formation (Grotzinger et al., 2014, 2015; Caswell and Milliken 2017; Young and Chan, 2017), and  $CaSO_4$ -filled veins also run along most of the OS ridges, so burial-related hydraulic fracturing may be considered a potential mechanism for the origin of the ridges. However, cross-cutting relationships indicate that the ridges and their infilling materials were lithified prior to the formation of sulfate-filled fractures; sulfate-filled fractures cross-cut some ridges and are not visible along all ridges (Figs. 2C and 2E). Moreover, hydraulic fracturing should yield relatively consistent fracture orientations (Hubbert and Willis, 1972), which are not observed at OS or SC. Zones of weakness created by early sediment-filled fractures were likely overprinted by burial-related stresses (Caswell and Milliken, 2017), followed by precipitation of calcium sulfates.

The ridges are restricted to the red surfaces and their associated fractures terminate at the boundary with the underlying sandstone, consistent with desiccation of a thin mud layer. This

TABLE 1. CHEMCAM MEASUREMENTS ON AND AROUND OLD SOAKER ROCK SLAB, MARS

Target	No. Points or Targets	SiO <sub>2</sub>	TiO <sub>2</sub>	Al <sub>2</sub> O <sub>3</sub>	FeO	MgO	CaO	Na <sub>2</sub> O	K <sub>2</sub> O	Sum of oxides (wt%)	Comments
Murray mudstones	88 targets	52.4	0.98	12.3	19.0	5.5	2.7	2.7	1.2	96.8	Sol 1410–1520
	std. dev.	2.1	0.05	1.4	1.0	1.1	0.9	0.4	0.3	2.3	
Red layer (3)	70 points	51.6	0.95	13.9	19.0	5.9	1.8	3.0	0.9	97.0	–
	std. dev.	1.6	0.07	1.5	1.5	0.6	0.4	0.4	0.4	2.5	
Gray layer (2)	12 points	49.8	0.93	11.7	19.1	5.8	1.4	2.8	2.2	93.9	Slightly low sum. One Cl line.
	std. dev.	1.4	0.15	1.7	0.9	0.7	0.5	0.5	0.5	1.9	
Bright layer (1)	12 points	39.8	0.86	8.8	12.5	3.0	17.1	1.5	0.4	84.0	Frequent S lines. Local F. Low sum.
	std. dev.	5.2	0.30	1.8	2.2	0.6	3.4	0.4	0.3	5.7	
Dark ridges	13 points	47.6	0.94	11.3	19.3	4.8	1.6	2.4	1.8	89.9	Low total. High H line.
	std. dev.	2.4	0.19	0.9	0.7	0.7	0.9	0.3	0.5	3.0	
Gilley Field Dark Spot	3 points	44.1	0.86	10.4	24.6	4.4	1.2	2.6	0.4	88.4	Low total.
	std. dev.	2.0	0.01	0.7	4.0	0.6	0.1	0.2	0.1	1.0	
Light vein	1 point	2.5	0.20	0.7	5.6	2.7	31.2	0.5	0.0	43.5	Multiple S lines.

Note: Targets consist of multiple points. Points on each feature are obtained at various locations and averaged to give a mean chemistry close to bulk chemistry. The quantification is obtained from comparison with laboratory data on Earth. Volatiles difficult to identify with laser ablation techniques (S, Cl, P) are not quantified. Oxide wt% sums are not normalized, such that low totals highlight the presence of volatiles. Standard deviations are calculated from the number of points of each category to display the variability inside each category.

TABLE 2. KEY APXS MEASUREMENTS ON OLD SOAKER ROCK SLAB, MARS

Target	Na <sub>2</sub> O	MgO	Al <sub>2</sub> O <sub>3</sub>	SiO <sub>2</sub>	P <sub>2</sub> O <sub>5</sub>	SO <sub>3</sub>	Cl	K <sub>2</sub> O	CaO	TiO <sub>2</sub>	Cr <sub>2</sub> O <sub>3</sub>	MnO	FeO <sub>T</sub>	Ni	Zn	Br
Thompson Island	2.62	5.96	9.13	44.80	1.00	6.29	2.38	0.83	3.75	1.01	0.32	0.18	21.39	749	645	1352
Error (±)	0.14	0.17	0.19	0.54	0.07	0.08	0.03	0.04	0.04	0.03	0.01	0.01	0.26	40	20	40
Fresh Meadow	3.22	5.86	7.54	34.04	0.87	13.34	2.51	2.29	3.95	0.75	0.33	0.20	24.83	477	405	927
Error (±)	0.14	0.17	0.19	0.43	0.05	0.15	0.04	0.07	0.04	0.03	0.01	0.01	0.26	25	15	30

Note: Alpha-particle X-ray spectrometer (APXS) oxide wt% or ppm concentrations of two representative measurements on Old Soaker. "Thompson Island" was acquired on the red bed (Sol 1566, SH -41.6 °C, FWHM (full width at half maximum) 146 eV, duration 8:09:16). Fresh Meadow was acquired on the underlying gray bed (Sol 1570, SH -20.7 °C, FWHM 169 eV, duration 1:26:11).

style of termination is inconsistent with synaeresis cracking or hydraulic fracturing, which in the latter case would also be expected to cross-cut the bedding planes (Hubbert and Willis, 1972; Plummer and Gostin, 1981; Young and Chan, 2017). The 0.5–3.5 cm length scale of the polygons on OS and SC is consistent with a millimeter- to centimeter-thick deformable layer, similar to the observed thickness of the red mudstone bed and analogous to terrestrial experiments (e.g. Shorlin et al., 2000). Variation in polygon size across slabs may be due to changes in basal friction, bed thickness, or impurities. The cracks are parallel-sided (do not taper downward) in profile (Fig. 4), which can occur if the coupling between the desiccated and underlying beds is low enough to not affect the fractures (Shorlin et al., 2000).

### Lithification of Ridges

The ridges likely formed via desiccation of a surficial mud layer and filling by sediment sourced from an overlying bed. Although the ridges and underlying gray bed are compositionally similar, the occurrence of interstratified gray and red beds suggests that a gray mudstone originally covered the cracked red mudstone and acted as a source of fracture fill material. Diagenesis associated with later fluids may account for their current similar compositions. Sulfates and other salts may have formed during desiccation as evaporites and/or after the fractures lithified. After deposition, the Murray formation was buried under up to several kilometers of sediment that likely provided sufficient overburden pressure to generate hydraulic fractures (Caswell and Milliken, 2017; Young and Chan, 2017). These fractures likely propagated along pathways of reduced strength produced by the desiccation cracks, and in some cases cross-cut polygons. These fracture networks then acted as conduits for fluid precipitation of CaSO<sub>4</sub> cements.

### CONCLUSIONS AND IMPLICATIONS FOR GALE CRATER PALEOLAKES

Recognition of distinct suites of sedimentary structures is a powerful tool in interpreting Mars paleoenvironmental history as it has been for Earth. The Murray formation is interpreted to record a transition from long-lived (~10<sup>5</sup>–10<sup>7</sup> yr) perennial lacustrine conditions observed in the basal Murray (Grotzinger et al., 2015; Hurowitz et al., 2017) to episodically exposed conditions recorded by the desiccation-cracked surfaces in the Sutton Island member of the Murray. The

predominance of T-junctions at OS and SC indicates a single drying event rather than multiple cycles of wetting and drying. The identification of desiccation cracks is an important facies attribute of the Murray formation that suggests a history of oscillating lake levels that led to intermittent exposure and possible evaporative diagenesis. The drier conditions may represent a temporal transition from deeper lacustrine facies dominated by suspension fallout to shallower lakes with more common traction deposition and desiccation. The Sutton Island member is ~70 m stratigraphically higher than the Pahrump Hills member, but is also >1 km closer to the center of the Gale lake basin. This suggests the exposed lake facies are not basin margin facies, but rather lowstand facies which represent lake level oscillations.

### ACKNOWLEDGMENTS

We are indebted to the Mars Science Laboratory (MSL) project engineering and science teams, and MSL team members who participated in tactical and strategic operations, for their efforts that were vital in collecting the data presented. Thanks to S. Kattenhorn, K. Benison, and K. Herkenhoff for reviews that improved this manuscript. Some of this research was performed at the Jet Propulsion Laboratory, California Institute of Technology (USA), under a contract with NASA. This material is based upon work supported by the National Science Foundation Graduate Research Fellowship Grant No. DGE-1144469. These data are archived in the Planetary Data System (pds.nasa.gov).

### REFERENCES CITED

- Banham, S.G., et al. 2018, Ancient martian aeolian processes and palaeomorphology reconstructed from the Stimson formation on the lower slope of Aeolis Mons, Gale crater, Mars: *Sedimentology*, <https://doi.org/10.1111/sed.12469> (in press).
- Caswell, T.E., and Milliken, R.E., 2017, Evidence for hydraulic fracturing at Gale crater, Mars: Implications for burial depth of the Yellowknife Bay formation: *Earth and Planetary Science Letters*, v. 468, p. 72–84, <https://doi.org/10.1016/j.epsl.2017.03.033>.
- Edgar, L.A., Grotzinger, J.P., Hayes, A.G., Rubin, D.M., Squyres, S.W., Bell, J.F., and Herkenhoff, K.E., 2012, Stratigraphic architecture of bedrock reference section, Victoria Crater, Meridiani Planum, Mars, in Grotzinger, J.P., ed., *Sedimentary Geology of Mars: Society for Sedimentary Geology Special Publications*, v. 102, p. 195–209, <https://doi.org/10.2110/pec.12.102.0195>.
- El-Maarry, M.R., Watters, W., McKeown, N.K., Carter, J., Noe Dobrea, E., Bishop, J.L., Pommerol, A., and Thomas, N., 2014, Potential desiccation cracks on Mars: A synthesis from modeling, analogue-field studies, and global observations: *Icarus*, v. 241, p. 248, <https://doi.org/10.1016/j.icarus.2014.06.033>.
- Fedo, C. et al., 2017, Facies analysis and basin architecture of the upper part of the Murray formation, Gale Crater, Mars: 48<sup>th</sup> Lunar and Planetary Science Conference, The Woodlands, Texas, 19–23 March 2018, abs. 1689.
- Goehring, L., Conroy, R., Akhter, A., Clegg, W.J., and Routh, A.F., 2010, Evolution of mud-crack patterns during repeated drying cycles: *Soft Matter*, v. 6, p. 3562–3567, <https://doi.org/10.1039/B922206E>.
- Grotzinger, J.P., et al., 2005, Stratigraphy and sedimentology of a dry to wet eolian depositional system, Burns formation, Meridiani Planum, Mars: *Earth and Planetary Science Letters*, v. 240, p. 11–72, <https://doi.org/10.1016/j.epsl.2005.09.039>.
- Grotzinger, J.P., et al., 2014, A habitable fluvio-lacustrine environment at Yellowknife Bay, Gale Crater, Mars: *Science*, v. 343, <https://doi.org/10.1126/science.1242777>.
- Grotzinger, J.P., et al., 2015, Deposition, exhumation, and paleoclimate of an ancient lake deposit, Gale crater, Mars: *Science*, v. 350, <https://doi.org/10.1126/science.aac7575>.
- Hubbert, M.K., and Willis, D.G., 1972, Mechanics of hydraulic fracturing: *Transactions of the American Institute of Mining and Metallurgical Engineers*, v. 210, p. 153–166.
- Hurowitz, J.A., et al., 2017, Redox stratification of an ancient lake in Gale Crater, Mars: *Science*, v. 356, <https://doi.org/10.1126/science.aah6849>.
- Mangold, N. et al., 2017, ChemCam analysis of aqueous processes on polygonal cracks at Gale Crater, Mars: 48<sup>th</sup> Lunar and Planetary Science Conference, The Woodlands, Texas, 19–23 March 2018, abs. 1908.
- Nachon, M., et al., 2017, Chemistry of diagenetic features analyzed by ChemCam at Pahrump Hills, Gale crater, Mars: *Icarus*, v. 281, p. 121–136, <https://doi.org/10.1016/j.icarus.2016.08.026>.
- Plummer, P.S., and Gostin, V.A., 1981, Shrinkage cracks; Desiccation or synaeresis?: *Journal of Sedimentary Petrology*, v. 51, p. 1147–1156.
- Rampe, E.B., et al., 2017, Mineralogy of an ancient lacustrine mudstone succession from the Murray formation, Gale crater, Mars: *Earth and Planetary Science Letters*, v. 471, p. 172–185, <https://doi.org/10.1016/j.epsl.2017.04.021>.
- Shorlin, K.A., de Bruyn, J.R., Graham, M., and Morris, S.W., 2000, Development and geometry of isotropic and directional shrinkage-crack patterns: *Physical Review E: Statistical Physics, Plasmas, Fluids, and Related Interdisciplinary Topics*, v. 61, p. 6950–6957, <https://doi.org/10.1103/PhysRevE.61.6950>.
- Sletten, R.S., Hallet, B., and Fletcher, R.C., 2003, Resurfacing time of terrestrial surfaces by the formation and maturation of polygonal patterned ground: *Journal of Geophysical Research: Planets*, v. 108, p. 8044, <https://doi.org/10.1029/2002JE001914>.
- Williams, R.M.E., et al., 2013, Martian fluvial conglomerates at Gale Crater: *Science*, v. 340, p. 1068–1072, <https://doi.org/10.1126/science.1237317>.
- Young, B.W., and Chan, M.A., 2017, Gypsum veins in Triassic Moenkopi mudrocks of southern Utah: Analogs to calcium sulfate veins on Mars: *Journal of Geophysical Research: Planets*, v. 122, p. 150–171.

Manuscript received 18 December 2017  
 Revised manuscript received 20 March 2018  
 Manuscript accepted 29 March 2018

Printed in USA